metals

MDPI

Article

Precipitation Criterion for Inhibiting Austenite Grain Coarsening during Carburization of Al-Containing 20Cr Gear Steels

Huasong Liu [1], Yannan Dong [1], Hongguang Zheng [2], Xiangchun Liu [2], Peng Lan [1], Haiyan Tang [1] and Jiaquan Zhang [1,*]

[1] School of Metallurgical and Ecological Engineering, University of Science and Technology Beijing, Beijing 100083, China; liuhuasong_ustb@163.com (H.L.); ustb_dyn0801@163.com (Y.D.); lanpeng@ustb.edu.cn (P.L.); tanghaiyan@metall.ustb.edu.cn (H.T.)

[2] Central Research Institute of Baoshan Iron and Steel Co., Ltd., Shanghai 201900, China; zhenghongguang@baosteel.com (H.Z.); liuxiangchun@baosteel.com (X.L.)

* Correspondence: jqzhang@metall.ustb.edu.cn

Abstract: AlN precipitates are frequently adopted to pin the austenite grain boundaries for the high-temperature carburization of special gear steels. For these steels, the grain coarsening criterion in the carburizing process is required when encountering the composition optimization for the crack-sensitive steels. In this work, the quantitative influence of the Al and N content on the grain size after carburization is studied through pseudocarburizing experiments based on 20Cr steel. According to the grain structure feature and the kinetic theory, the abnormal grain growth is demonstrated as the mode of austenite grain coarsening in carburization. The AlN precipitate, which provides the dominant pinning force, is ripened in this process and the particle size can be estimated by the Lifshitz−Slyosov−Wagner theory. Both the mass fraction and the pinning strength of AlN precipitate show significant influence on the grain growth behavior with the critical values indicating the grain coarsening. These criteria correspond to the conditions of abnormal grain growth when bearing the Zener pinning, which has been analyzed by the multiple phase-field simulation. Accordingly, the models to predict the austenite grain coarsening in carburization were constructed. The prediction is validated by the additional experiments, resulting in accuracies of 92% and 75% for the two models, respectively. Finally, one of the models is applied to optimize the Al and N contents of commercial steel.

Keywords: gear steel; AlN precipitate; carburization; austenite grain size; Zener pinning; precipitation criterion

Citation: Liu, H.; Dong, Y.; Zheng, H.; Liu, X.; Lan, P.; Tang, H.; Zhang, J. Precipitation Criterion for Inhibiting Austenite Grain Coarsening during Carburization of Al-Containing 20Cr Gear Steels. *Metals* **2021**, *11*, 504. https://doi.org/10.3390/met11030504

Academic Editor: Andrea Di Schino

Received: 10 February 2021
Accepted: 15 March 2021
Published: 18 March 2021

1. Introduction

Gear steels include carbon structural steel (such as Q235), low-alloy high-strength structural steel (such as Q345), high-quality carbon structural steel (such as 45 steel), alloy structural steel (such as 40MnB and 42CrMo), and structural steel with guaranteed hardenability (such as 20CrMnTi and 20CrMo), etc. For the heavy-duty gear steels including 20CrMnTi, Cr-Mo and Cr-Ni-Mo series, carburizing and quenching treatments are required before usage. In the carburizing process, the austenite grains are prone to grow up, which affects the tensile strength, elongation, impact toughness [1–3], heat treatment distortion [4], and fatigue crack resistance [5,6] of the gears. To inhibit austenite grain coarsening, the presence of certain nanoscale particles is needed to achieve the pinning on the austenite grain boundary (GB) [7]. Common gear steels use AlN as the pinning particles, of which the carburizing temperature is in the range of 930–980 °C. A higher carburizing temperature requires the addition of Nb or Nb−Ti microalloying elements [8,9].

Although high-temperature carburizing has the advantages of increasing the carburized layer thickness and shortening the carburizing time, the commercial gear steels mostly

use AlN to pin the austenite GB at present. The adequate acid-soluble Al and N in steel can guarantee the control of austenite grain size during carburizing. However, for the gear steel grades containing peritectic or hypo-peritectic composition, the excessive addition of Al or N may cause the surface crack problem in continuous casting production. For instance, in several Chinese plants, the production of 20Cr, 20CrMo, and 20CrMnTi has suffered frequent surface or corner cracks for a long time. Reducing the content of Al or N is conducive to improving the third brittle zone of the slab surface [10]. Hence the composition design has to balance the requirements of carburization and the suppression of continuous casting cracks. For this purpose, the quantitative relationship between the Al and N content and the austenite grain size after carburization is required. Work has been carried out to investigate this relationship. Militzer et al. studied the austenite grain growth kinetics in Al-killed plain carbon steels and found that the grain growth depended strongly on the degree of AlN precipitation [11]. Pous-Romero et al. studied the austenite grain growth in a nuclear pressure vessel steel of which the pinning particle was determined as AlN [12]. Two regimes of grain growth were reported to be produced due to the existence or dissolution of precipitates. Other experimental works also manifested that high contents of Al and N were beneficial for obtaining the fine austenite grain structure and avoiding abnormal grain coarsening [13]. However, the precise criterion of composition or AlN precipitation has not been reported to date, resulting in uncertainty in the reduction of Al or N content for crack-sensitive steels.

The present work aims to reveal the criterion of austenite grain size control in the carburization of Al-bearing gear steels. Six compositions with various Al and N contents were designed based on the commercial 20Cr steel, and the pseudocarburizing experiments were carried out in the temperature range of 977–1019 °C. Combining with the AlN precipitation behavior, the dependence of grain growth behavior on the precipitate condition was revealed. After determining the grain coarsening mode in carburization, the critical condition for abnormal grain growth was obtained by the multiple phase-field (MPH) simulation. Finally, the models for predicting the grain coarsening were proposed and validated by additional experiments.

2. Materials and Methods

2.1. Material

A typical gear steel grade 20Cr was investigated in this work, which suffers great crack sensitivity in the continuous casting procedure. To investigate the effect on the grain growth behavior of Al and N contents, six steel compositions were designed, based on the commercial 20Cr steel. The raw materials were melted in a 180 Kg vacuum induction furnace and cast into an ingot with a section of 170 × 170 mm^2. Then the cooled casts were hot-forged to the bars with a section of 34 × 34 mm^2, which started at 1200 °C and air-cooled to room temperature after the deformation. Finally, the pseudocarburizing test specimens were machined from the bars with a size of 12 × 12 × 15 mm^3 of which the long axis was parallel to the deformation direction. The precise composition of each bar was measured at a quarter of the thickness, and the results are listed in Table 1. It was found that the contents of main solutes except Al and N were rather stable, and the contents of Ti and Nb were all trace except for the S3. The metallographic structure of S1 in the cross-section is shown in Figure 1, which was composed of polygonal ferrite and pearlite at room temperature.

2.2. Experiments

The pseudocarburizing experiments were carried out in a high-temperature resistance furnace. Since the practical carburizing temperature is in the range of 950–980 °C for 20Cr, the experimental carburizing temperatures were set as 977, 998, and 1019 °C, which covered the highest carburizing temperature of the current Al-containing gear steels. The carburizing time was chosen as 4 h. Once finished carburizing, the samples were taken out from the furnace and water-quenched immediately. The furnace temperature was

calibrated by the platinum and rhodium 10-platinum thermocouple, and argon gas was continuously blown into the furnace to reduce oxidation during the experiment.

Table 1. Chemical compositions of the experimental steels (wt.%).

Steel	C	Si	Mn	S	Cr	Ni	Ti	Nb	Al	N
S1	0.21	0.32	0.88	0.002	1.23	0.16	<0.005	<0.0005	0.028	0.0183
S2	0.22	0.31	0.88	0.002	1.22	0.16	0.0023	<0.0005	0.019	0.015
S3	0.21	0.3	0.88	0.002	1.22	0.15	0.013	0.0007	0.029	0.0115
S4	0.21	0.3	0.85	0.002	1.2	0.16	<0.0005	<0.0005	0.014	0.015
S5	0.21	0.32	0.87	0.002	1.2	0.17	0.0005	<0.0005	0.01	0.011
S6	0.22	0.31	0.89	0.002	1.21	0.15	0.0012	0.0005	0.018	0.0065

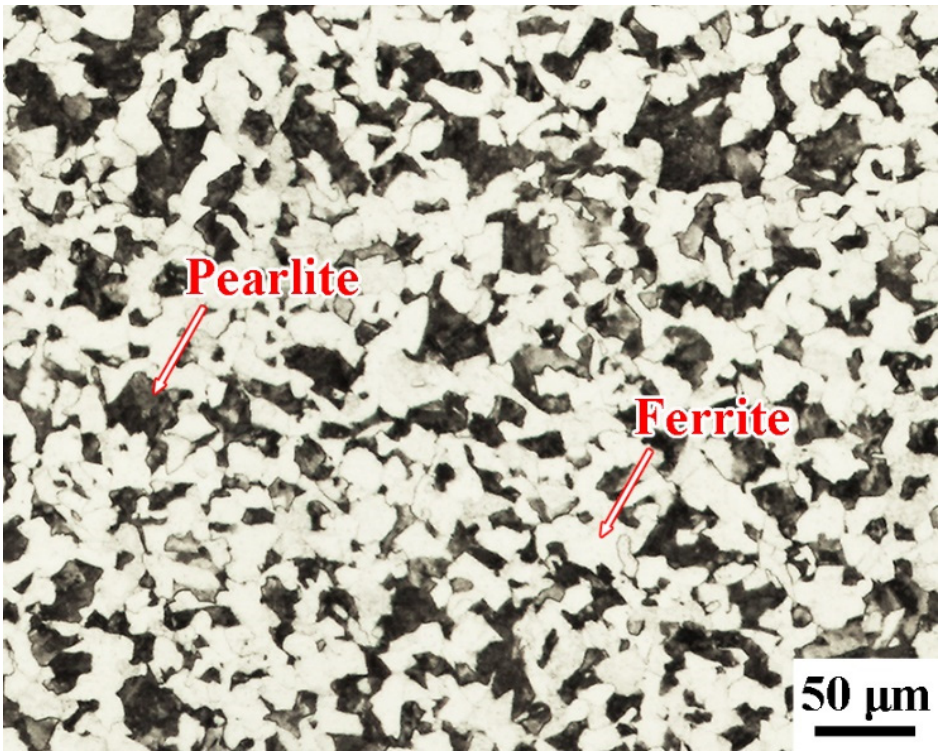

Figure 1. The microstructure of S1 at room temperature.

To further avoid the influence of surface oxidation, the middle section of each sample was used as the surface for microstructure characterization. The section was polished to 0.5 μm and etched by the saturated picric acid aqueous solution to reveal the original austenite GBs. The prior austenite grain structure (PAGS) was photographed and collected by an optical microscope (UOP, Chongqing, China), and the grain size was measured by the area equivalent diameter. Each sample was measured to at least 1500 (when the grains were fine) or 500 (when the grains were coarse) grains. Using the carbon replication method, the morphology and composition of the precipitates in some samples were detected by a transmission electron microscope (TEM, Oxford Instruments, Abingdon, UK) and an attaching energy dispersive spectrometer (EDS, Oxford Instruments, Abingdon, UK).

2.3. Precipitation Model

The mass fraction of precipitation was calculated by the commercial software Thermo-Calc using the TCFE-v8.1 database (2017, Thermo-Calc Software, Stockholm, Sweden), and

the mean radius of AlN particles was estimated through the classical Lifshitz−Slyosov−Wagner (LSW) theory [14]

$$r_p = \left(r_0^3 + \frac{8\sigma_I C D V_m^2}{9RTV_B}t\right)^{1/3} \quad (1)$$

where σ_I is the surface energy of the particle−matrix interface, V_m the precipitate molar volume, C the equilibrium mole fraction of solute Al in the matrix, D the bulk diffusion coefficient of solute Al in austenite, V_B the mole volume of solute Al, R the gas constant, T and t the absolute temperature and ripening time, respectively. The initial radius of the AlN particle r_0 was set as 7.5 nm in the calculation, which had very little influence on the result. The mole fraction C was obtained by the solubility product K_γ of AlN in austenite.

2.4. MPH Method

A two-dimensional polycrystalline phase-field model was selected to analyze the occurrence condition of abnormal grain growth. This model uses the order parameter φ_i to describe the probability that a spatial point belongs to the grain orientation i, where $\varphi_i = 1$ (0) means it is located in the grain (outside the grain), and $\varphi_i = 0$~1 means it is located at the GB. For a system containing less than Q grains, i.e., $i = 1, 2 \ldots Q$, the order parameter of each point must satisfy $\sum_1^Q \varphi_i = 1$. That is, each spatial point can only locate either inside a grain or at the GB of multiple grains. The order parameter evolution is calculated by [15]

$$\begin{gathered} \frac{\partial \varphi_i}{\partial t} = -\frac{2}{n}\sum_{j\neq i}^{n} L_{ij}\left(\frac{\delta F}{\delta \varphi_i} - \frac{\delta F}{\delta \varphi_j}\right) \\ \frac{\delta F}{\delta \varphi_j} = \sum_{i\neq j}^{n}\left(\frac{\varepsilon_{ij}^2}{2}\nabla^2\varphi_i + \omega_{ij}\varphi_i\right) \\ \omega_{ij} = \frac{4\sigma_{ij}}{W_{ij}}, \varepsilon_{ij}^2 = \frac{8W_{ij}\sigma_{ij}}{\pi^2}, L_{ij} = \frac{\pi^2 m_{ij}}{8W_{ij}} \end{gathered} \quad (2)$$

where n is the total number of grain orientations existing at a certain point, σ_{ij}, m_{ij}, and W_{ij} the GB energy, GB mobility, and GB thickness between grains i and j, respectively. In this simulation, the anisotropy of these parameters is all ignored.

The Zener pinning of the precipitate particle is required in the simulation of abnormal grain growth, which is introduced by modifying the GB mobility [16]

$$m_{ij} = \begin{cases} m_{ij}^0 \exp\left(-\frac{0.12P_z}{|\Delta G_{ij}| - P_z}\right) & \text{if } |\Delta G_{ij}| > P_z \\ 0.01 m_{ij}^0 & \text{else} \end{cases} \quad (3)$$

where ${m_{ij}}^0$ is the GB mobility without pinning, P_z the particle pinning force. The driving force of the GB between grains i and j is obtained by the grain diameters d_i and d_j [17]

$$|\Delta G_{ij}| = 2\sigma_{ij}\left|\frac{1}{d_i} - \frac{1}{d_j}\right| \quad (4)$$

The initial grain structure in MPH simulation was generated by randomly placing the circular nuclei with the size distribution obeying the log-normal function

$$f(d) = \frac{1}{ds\sqrt{2\pi}}\exp\left[-\frac{(\ln d - \mu)^2}{2s^2}\right] \quad (5)$$

where d is the grain diameter, μ and s the mean and standard deviation of ln d, respectively. The MPH simulations were carried out on a personal computer with Matlab (2016b, Mathworks, Natick, MA, USA) language, and the number of grid points is 801 × 801. All the parameters used in this simulation and LSW calculation are given in Table 2.

Table 2. Parameters in the multiple phase-field (MPH) simulation and Lifshitz−Slyosov−Wagner (LSW) calculation.

Parameter	Value	Reference
Grid space Δx	$\exp(\mu)/20$	-
Time step Δt	$0.9\Delta x^2/(4L_{ij}\varepsilon_{ij}^2)$	-
W_{ij}	$6\Delta x$	-
σ_{ij}	0.5, J/m^2	-
m_{ij}^0	0.5×10^{-12}, m^4/(J·s)	-
σ_I	0.75, J/m^2	[18]
D	$0.000251\exp(-253{,}400/RT)$, m^2/s	[19]
V_m	1.33×10^{-5}, m^3/mol	[18]
V_B	1.05×10^{-5}, m^3/mol	[1]
K_γ	$\exp(4.5985–11{,}568/T)$	[19]

[1] The mole volume of solute Al is estimated by the density of Al at 600 °C.

3. Results

3.1. Initial Austenite Grain Structure

The PAGS after holding 300 s at a carburizing temperature was regarded as the initial grain structure of carburization. Taking S2 as an instance, the initial grain structure of 977 °C carburizing is shown in Figure 2a. The austenite grains were uniform and fine before coarsening. Figure 2b gives the frequency distribution of grain size of S1, S2, and S4 when holding at different temperatures for 300 s. Although the carburizing temperatures were different, the initial grain structures were close in these cases. The size distributions could be well fitted by the log-normal distribution function in Equation (5). It should be pointed out that, when the contents of Al and N were very low, the coarse grains were formed even after holding 300 s at high temperatures, such as S6 carburizing at 1019 °C. According to the other cases, the average grain size at the start of each carburization could be determined as about 12 μm.

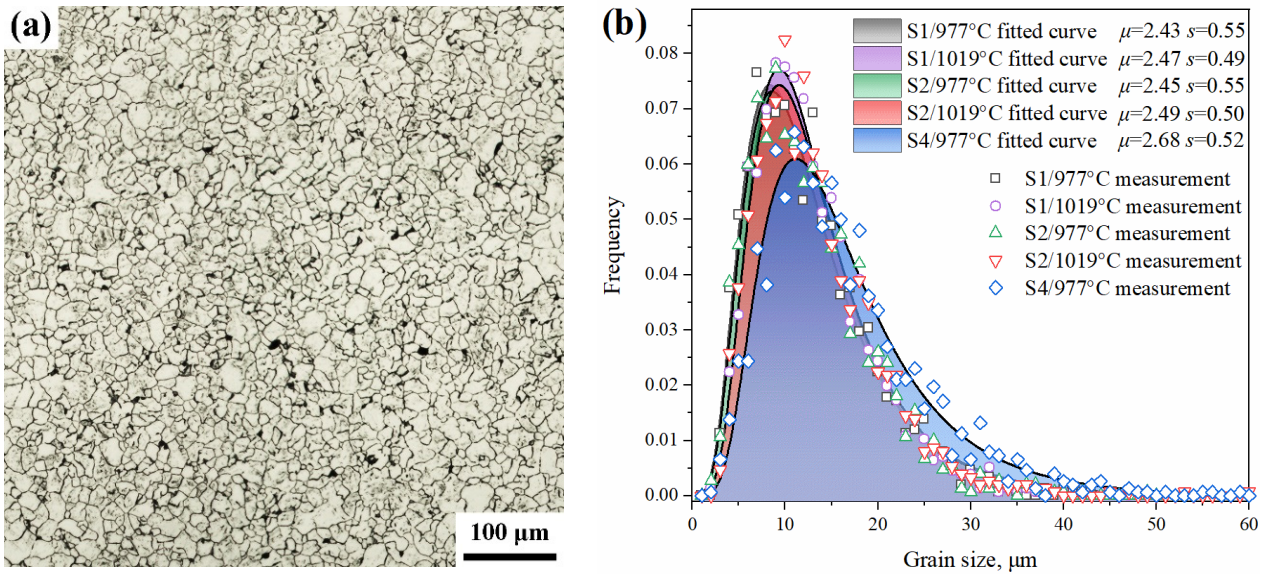

Figure 2. (**a**) Prior austenite grain structure (PAGS) after holding 300 s at 977 °C of S2; (**b**) Grain size-frequency distributions after holding 300 s at various temperatures of S1, S2, and S4.

3.2. PAGS after Pseudocarburization

The PAGSs after 977 °C pseudocarburization are shown in Figure 3. With the same carburizing scheme, quite different PAGSs were developed. Due to the high contents of

Al and N in S1, S2, and S3, the austenite grains remained fine after carburizing, which nearly maintained the initial state shown in Figure 2a. For the other steels, of which the Al or N content was low, very coarse grains were formed. In these cases, as shown in Figure 3b,c, the grain coarsening was quite inhomogeneous. As a result, the coarse- and fine-grain regions were divided apparently, which was an indication of the abnormal grain growth [20]. With the decrease of Al or N content, the coarsening of PAGS became so severe that the fraction of the coarse-grain region increased. A similar phenomenon existed with the increase of carburizing temperature.

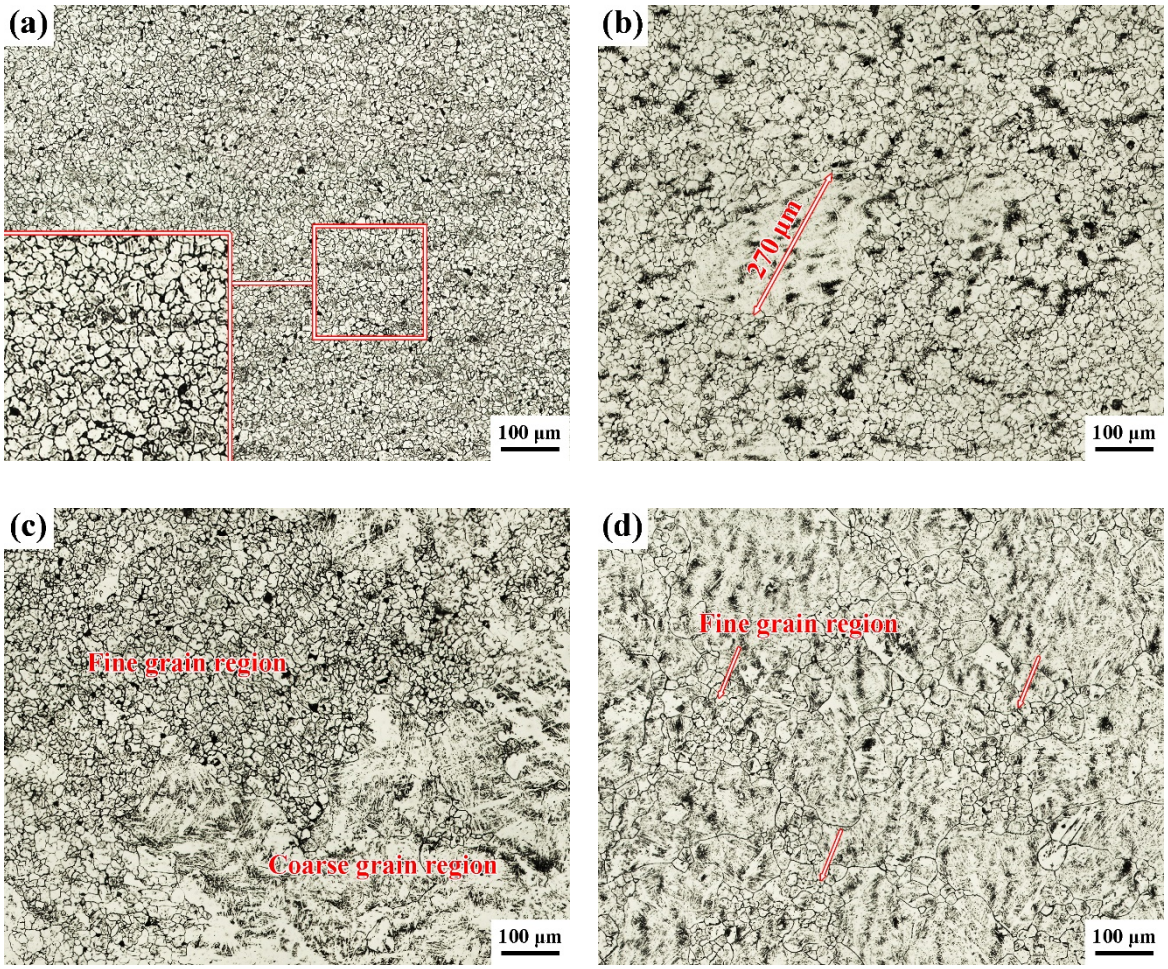

Figure 3. PAGSs after holding for 4 h at 977 °C of (**a**) S2, (**b**) S4, (**c**) S5, and (**d**) S6.

3.3. AlN Precipitation

Figure 4 shows the TEM micrograph and the EDS spectrum of the precipitate particles in S3 and S4 after the pseudocarburization at 977 °C. Due to the presence of Ti, the precipitates in S3 always contained Ti, of which the larger particles should be Al-rich (Ti,Al)(C,N) composite precipitates, while the fine particles were TiN or Ti-rich composite precipitates. However, bearing the trace content of Ti or Nb in other steels, the precipitates in S4 were mainly AlN particles and a few large MnS particles. The detection demonstrated that, during the high-temperature carburizing, the precipitates had undergone significant Ostwald ripening, resulting in the coarse particles more than 100 nm in size and the fine particles with sizes of only tens of nm. In this process, due to the higher N content and a certain amount of Ti in S3, the number of fine particles was higher than that of S4.

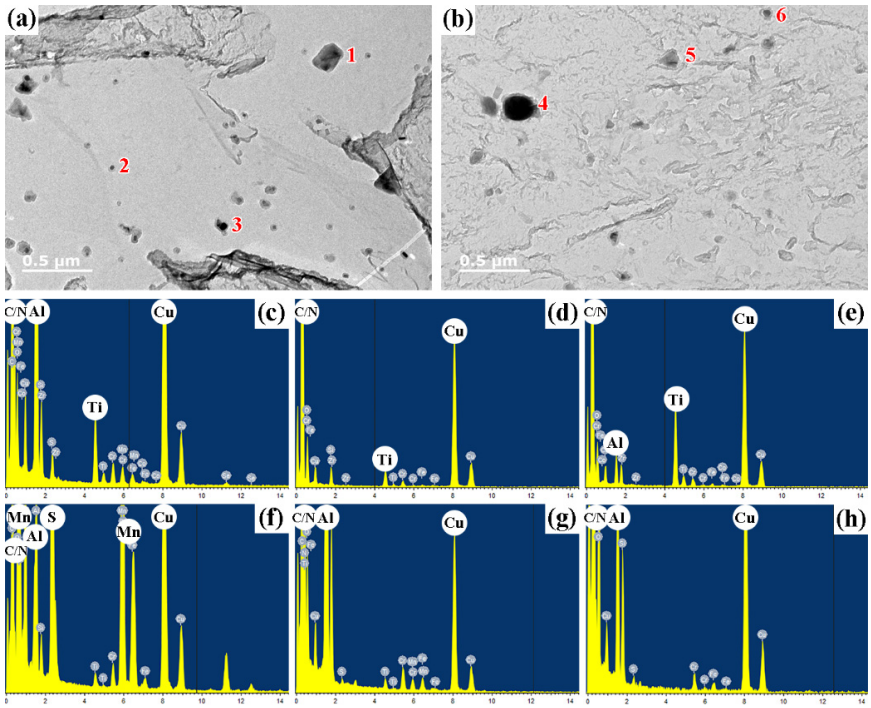

Figure 4. TEM micrograph of the precipitates after holding for 4 h at 977 °C of (**a**) S3 and (**b**) S4 and the corresponding EDS spectra of (**c**–**e**) particles 1–3 and (**f**–**h**) 4–6.

The calculated mass fraction of S1 equilibrium precipitation is shown in Figure 5a. In the range of 950–1050 °C, AlN was the main precipitate and only a small amount of TiN and MnS existed. So, the dominant pinning particle at the pseudocarburizing temperatures should be AlN as expected. Figure 5b plots the equilibrium mass fraction of this precipitate in various steels, and the sum fraction of AlN and TiN was added for S3 owing to the existence of Ti. As the contents of Al and N reduced, the initial precipitation temperature and the precipitation amount of AlN both decreased. The evolution of AlN particle radius during the carburization was then calculated by the LSW theory, and the results of carburizing at 977 and 1019 °C are shown in Figure 6. Interestingly, it was revealed that the influence of Al and N contents on the particle size was complicated and no monotonous relationship could be found. According to the TEM detections, the average AlN particle radius in S4 after the carburization at 977 °C was about 27.5 nm, which was very close to the calculation result of the kinetic model.

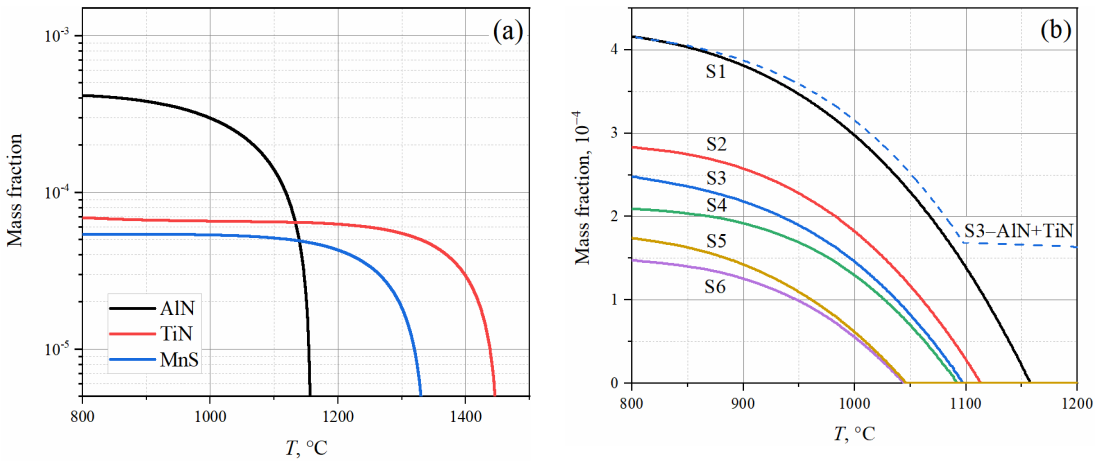

Figure 5. (**a**) Calculated equilibrium precipitation in S1; (**b**) equilibrium mass fractions of AlN in different steels.

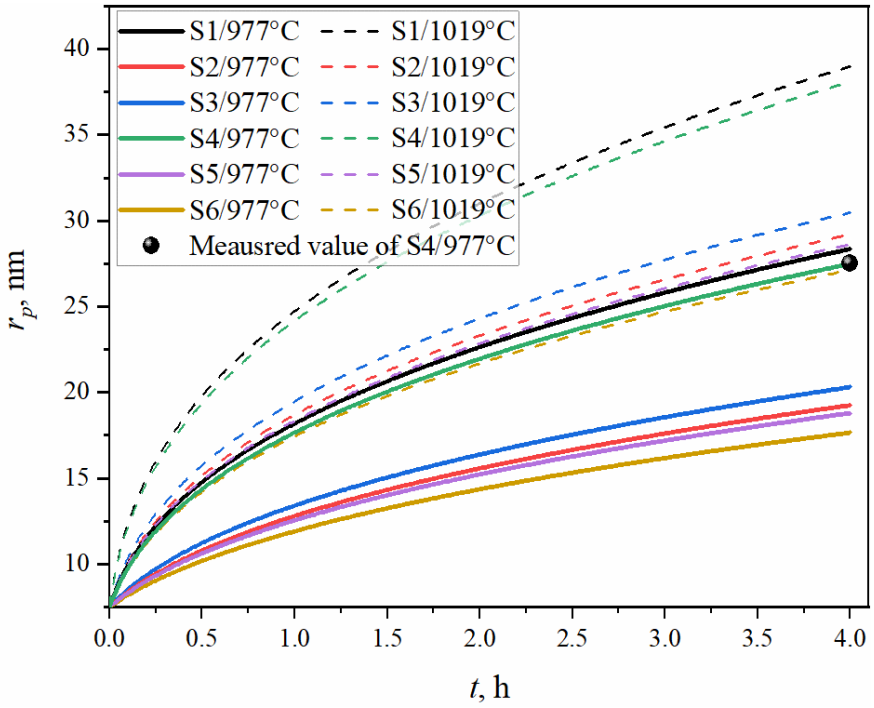

Figure 6. Calculated average radiuses of AlN particles as functions of time during carburizing at 977 and 1019 °C in various steels.

3.4. Relationship between the Precipitation and PAGS

The average grain size after carburization of each case is listed in Table 3. In these cases, the PAGSs of S1, S2, and S3 maintained the fine and uniform structure as shown in Figure 3a, while in those of S4, S5, and S6 appeared the huge grains as Figure 3b–d revealed. It was noted that the average grain size could only partly reflect the coarsening of PAGS. Taking S4 as an instance, although the huge grains were formed after carburizing at 977 and 998 °C, the average grain sizes remained close to the initial one because the number of coarse grains was far less compared to the number of fine grains.

Table 3. The average grain size of each case after pseudocarburization (μm).

Carburizing T (°C)	S1	S2	S3	S4	S5	S6
977	11.72	13	12.46	16	33.91	22.24
998	13.36	12.7	13.16	12.43	42.47	27.36
1019	11.46	13.69	13.23	33.03	57.5	41.78

The influence of precipitate amount on the PAGS after carburization was examined. The corresponding relationship is shown in Figure 7a. Considering the average grain size could not reflect the grain coarsening, the black square and red circular dots marked the fine PAGS and the PAGS containing coarse grains, respectively. A critical mass fraction between these two structures was revealed. Once the mass fraction was below the critical value, the huge grains appeared, and the average grain size increased as the precipitate amount decreased. Given the content of Ti in steels, especially in S3, the influence of TiN precipitation was also considered in Figure 7a through the sum fraction of TiN and AlN. However, when considering the TiN precipitation, the critical mass fraction for grain coarsening could be determined as about 1.56×10^{-4}. If using f_p/r_p (f_p is the volume fraction of precipitate) as the pinning strength of AlN particles, Figure 7b shows the relationship between pinning strength and PAGS feature. A similar result with Figure 7a is obtained, where the critical f_p/r_p is about 14,574 m^{-1}. Below this critical value, there exists an abnormal case with fine PAGS as circled in Figure 7b. For this case, the actual pinning

strength should be higher than the present value, because it belongs to S3 which should consider the pinning of TiN. The critical pinning strength corresponds to the carburizing case at 977 °C of S4. The indication can also be found in the associated PAGS in Figure 3b, where the matrix is still fine grains and the coarse grains are few and isolated.

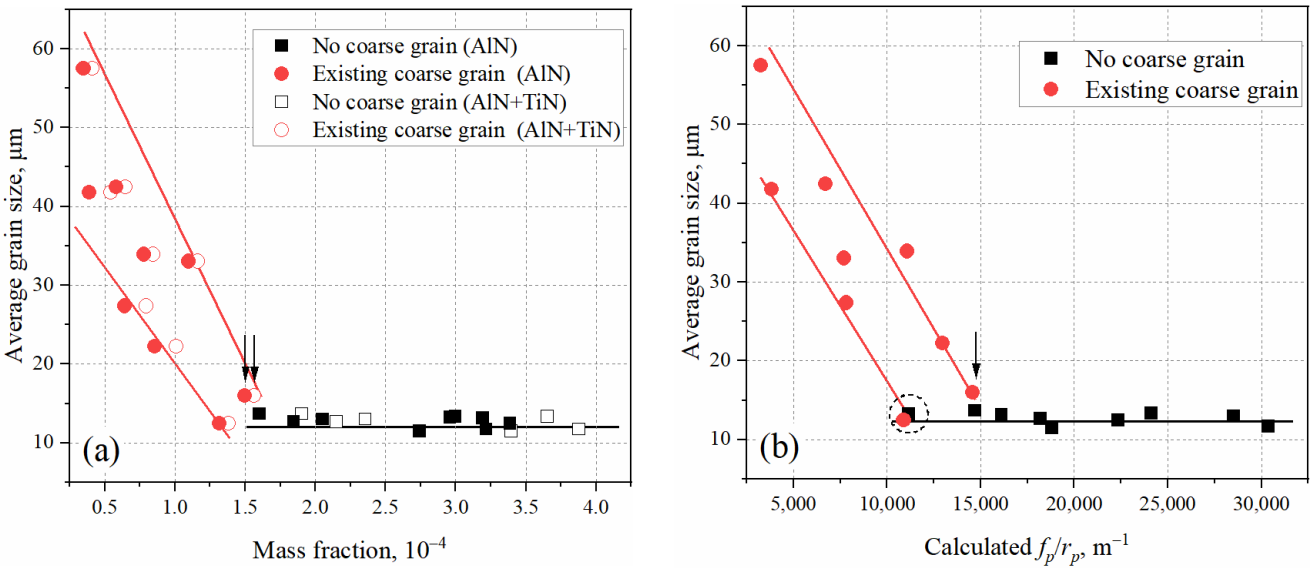

Figure 7. Relationships between the PAGS feature after carburization and the equilibrium mass fraction of precipitation (**a**) and the pinning strength f_p/r_p (**b**). In image (**b**), the circled dot corresponds to the case of S3 carburizing at 1019 °C.

4. Discussion

4.1. Grain Coarsening Mode in Carburization

The grain size distributions of S2 and S4 before and after the carburizing treatments are shown in Figure 8. It is seen that regardless of the occurrence of grain coarsening, the portion of fine grains remained almost unchanged during the carburization. The failure of the grain size control was the appearance of large grains, of which the size could reach dozens of times that of fine grains. This is an indication that the coarsening of PAGS should be carried out in an abnormal grain growth regime in carburization. The moving rate of austenite GB can be described as

$$v = m_0(P_0 - P_z - P_d) \tag{6}$$

where m_0 is the intrinsic GB mobility, P_0 the intrinsic driving force of GB migration. The solute dragging force P_d is related to the GB velocity v as [21]

$$P_d = \frac{avc}{1 + b^2v^2} \tag{7}$$

where a and b are the constants related to the binding energy and diffusion coefficient of the solute element at the GB, and c the bulk concentration of solute. When v is very low, P_d is almost a linear function of v. Therefore, Equation (6) is rewritten as

$$v = \frac{m_0}{1 + acm_0}(P_0 - P_z) = m(P_0 - P_z) \tag{8}$$

where m is the equivalent GB mobility considering the solute dragging which corresponds to the m_{ij}^0 in Equation (3).

When grain growth occurs, two distinct regimes exist, i.e., normal grain growth and abnormal grain growth. Almost all grains can have obvious GB motion in the former regime, while only part of the grains can grow up in the latter one. Many works have confirmed

that abnormal grain growth can be induced by the effect of particle pinning [16,17,20,22]. Besides, under the dragging force shown in Equation (7), the transition from the low-speed motion to the high-speed motion of GB was also expected to lead to abnormal grain growth [23]. However, the required driving force for this transition is extremely large and no experimental report has been found for the austenite grain in steel. So this paper was concerned only about the low-speed region of GB motion to obtain the equivalent mobility as shown in Equation (8). That means, only the particle pinning work is expected to cause abnormal grain growth. The driving force of GB migration is calculated by

$$P_0 = 2\sigma\kappa \tag{9}$$

where σ is the isotropous expression of σ_{ij}, κ the GB curvature. In a three-dimensional polycrystalline system, κ can be expressed as a function of the adjacent grain sizes $2|1/d_1 - 1/d_2|$ [24]. For a system with an average grain size of d_m, assuming the maximum grain size is $3d_m$, the driving force range of GB migration is about $(0, 8\sigma/3d_m)$ and the average driving force is about $2\sigma/3d_m$ [25]. Considering features of the grain growth regimes and according to Equation (8), when normal growth occurs, the Zener pinning force should be within $(0, 2\sigma/3d_m)$ so that most of the GBs can move. When abnormal growth occurs, the pinning force should be within $(2\sigma/3d_m, 8\sigma/3d_m)$, then only the GBs with a large size difference in neighboring grains can move. Nearly no grain growth occurs when the pinning force exceeds $8\sigma/3d_m$.

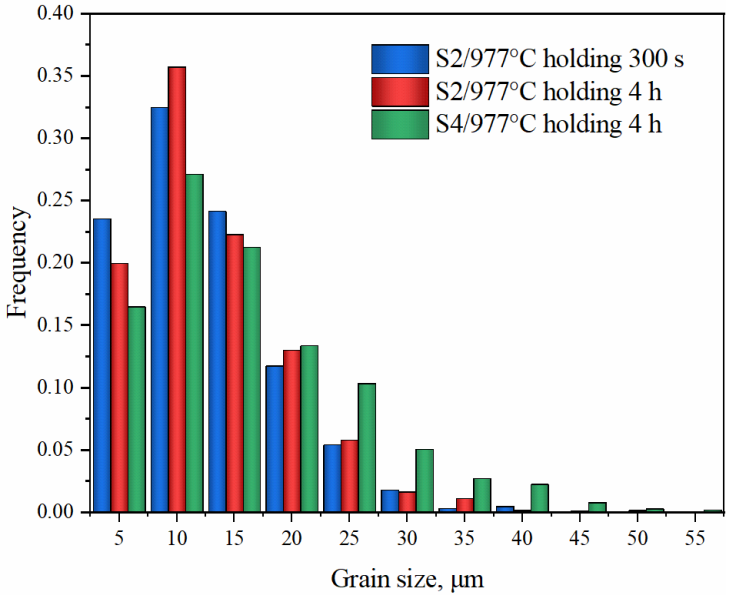

Figure 8. Comparison of austenite grain size-frequency distributions of S2 at the start of carburization and S2 and S4 after carburization at 977 °C.

During carburizing, the pinning work of precipitates has four possible situations: (1) the initial pinning force falls into $(0, 2\sigma/3d_m)$; (2) the initial pinning force falls into $(2\sigma/3d_m, 8\sigma/3d_m)$; (3) the pinning force is greater than $8\sigma/3d_m$ initially but falls into $(2\sigma/3d_m, 8\sigma/3d_m)$ after the dissolution and ripening; (4) the pinning force is always greater than $8\sigma/3d_m$. Among these situations, the austenite grains will grow up normally in case (1) or have an abnormal growth in cases (2) and (3). We should note that the occurrence of grain growth does not mean the failure of grain size control. After the normal grain growth, in case the mean grain size is less than the permissible value, the control of grain size is successful. However, for the gear steel that needs to be carburized, the precipitation in the steel aims to prevent the austenite grain growth which means the excessive precipitates are always designed. Therefore, the failure of grain size control should arise from the insufficient precipitates or the dissolution and Ostwald ripening of precipitates which

reduces the pinning force during carburizing. Then the pinning force is less than $8\sigma/3d_m$ and drops to the adjacent region of abnormal grain growth. Once the abnormal growth occurs, the coarsened grains will continue to grow up and develop huge sizes far exceeding the values permissible by the users. Therefore, the austenite grains can have two states in the carburizing process, i.e., no growth and abnormal growth, and the latter is the manifestation of grain coarsening. In our experiments, with the decreasing contents of Al and N, the pinning force would also decrease from the region associated with no grain growth. This is why the grain size variation had a discontinuity in Figure 7. The criterion between the no grain growth and the grain coarsening behaviors corresponds to the critical condition of abnormal grain growth.

4.2. Condition for Abnormal Grain Growth

To achieve the precise condition of abnormal grain growth, the MPF method was employed to simulate the various grain growth behaviors. According to Equation (8), the occurrence of abnormal growth is determined by the competition between P_z and P_d, which is independent of mobility. The particle pinning force can be calculated by

$$P_z = \xi \frac{\sigma \cdot f_p}{r_p} \tag{10}$$

where ξ is a dimensionless constant, determined by the particle shape, the geometric characteristics of the interface between the particle and the matrix, the coherence of the interface, and the connection properties [26]. Equations (9) and (10) show that both P_0 and P_z are linearly related to σ, so the occurrence of abnormal grain growth is also independent of the GB energy. In the MPH simulation, the mobility without pinning work ${m_{ij}}^0$ was assumed as 0.5×10^{-12} $m^4/(J{\cdot}s)$, and the GB energy σ was set as $0.5\ J/m^2$. When constructing the initial grain structure, the standard deviation was set as 0.33, and the average size was within 5–25 μm. It should be pointed out that, in the present model, if using the measured standard deviation of 0.52, the abnormal growth cannot occur. This may be because, with the wide grain size distribution, the coarsening grains are so many that the growth cannot continue due to the encounters, which indicates that the present particle pinning model of Equations (3) and (4) can be improved in the future.

The generated initial grain structure with an average size d_0 of 10 μm is shown in Figure 9a, which is similar to the actual initial grain structure in Figure 2a. After the simulations for 4 h carburizing, the relationship between the pinning force and the grain growth regime is achieved in Figure 10. It can be seen that under different initial sizes, three regimes of grain growth, i.e., normal growth, abnormal growth, and no growth can occur according to the pinning force. The upper bound condition of the abnormal grain growth was well fitted by the power function shown in Figure 10. Three simulated grain structures are given in Figure 9b,c for instance. The fine and uniform grain structure was obtained in the no grain growth regime, while the mixed one after abnormal grain growth was similar to the PAGS after carburization shown in Figure 3c,d.

4.3. Prediction of Grain Coarsening in Carburization

Figure 7a reveals that under experimental conditions, the precipitate mass fraction could be used as the critical condition of abnormal grain growth. The reason is, when the carburizing temperatures were close, the difference between the average sizes of AlN particles was not too much. Figure 11 shows the relationship between the mass fraction of AlN precipitate and the calculated AlN pinning strength after carburizing for 2 and 4 h. Although the particle sizes were different, the function between mass fraction and pinning strength was close to a linear one. Then the critical condition for abnormal grain growth could be presented by the former. Therefore, with the close carburizing temperature and time, the critical mass fraction of AlN precipitate can be used to avoid the occurrence of abnormal grain growth as

$$f_{p,m} > 1.56 \times 10^{-4} \tag{11}$$

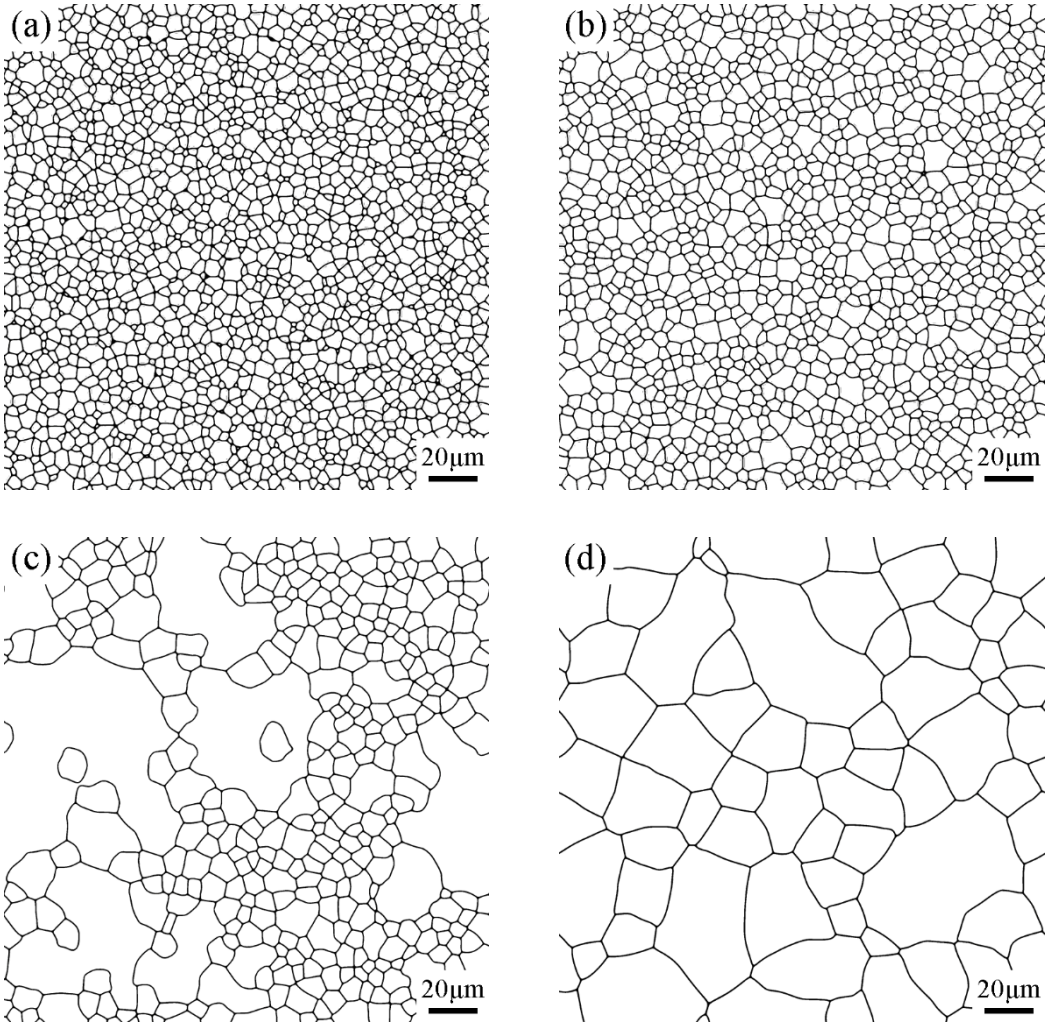

Figure 9. The initial grain structure in MPH simulation (**a**) and the final grain structures after simulated carburization with d_0 of 10 μm. Images (**b**–**d**) correspond to the cases of (**b**–**d**) in Figure 10.

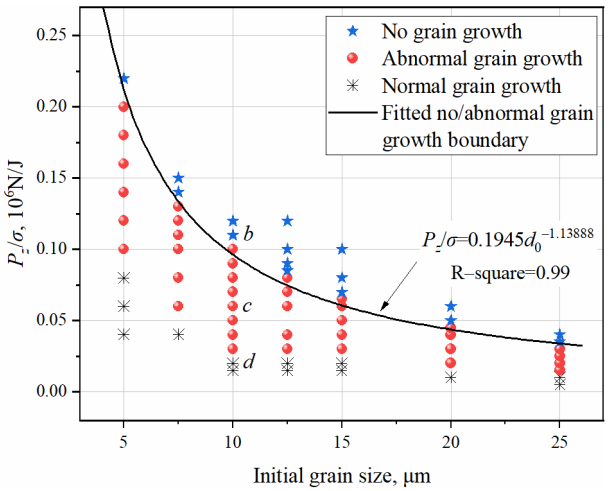

Figure 10. Various grain growth regimes as functions of initial grain size and pinning force.

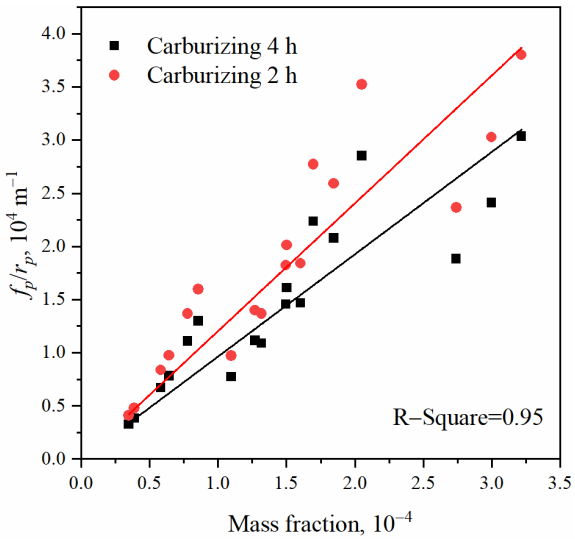

Figure 11. Relationship between the calculated pinning strength and the mass fraction of AlN precipitate.

However, in case the carburizing temperature or time changes much, the variation of AlN particle size needs to be considered. After the MPH simulation results as shown in Figure 10, the boundary of pinning force for abnormal grain growth can be predicted by

$$P_z = 0.1945 \cdot {d_0}^{-1.13888} \cdot \sigma \quad (12)$$

where d_0 is in the unit of m. Note that, the driving force of GB in a two-dimensional system is half of that in the actual three-dimensional system, as shown in Equations (4) and (9). Hence the critical pinning force in this equation needs to be doubled when applied in a three-dimensional system. With the initial grain size of 12 μm, the calculated critical P_z/σ is 156,377 m^{-1}. Combined with the critical pinning strength shown in Figure 7b, the dimensionless constant ξ can be determined from Equation (10) for the pinning of AlN particles on austenite GB. The obtained value of 10.73 is between 3/2 and 12 as recommended in the literature [27,28]. Then the critical condition for inhibiting the grain coarsening in carburization can be obtained as

$$\frac{f_p}{r_p} > 0.03625 \cdot {d_0}^{-1.13888} \quad (13)$$

The occurrence of abnormal grain growth depends on the competition between P_z and P_d of grain structure. If ignoring the variation of standard deviation in grain size distribution and assuming the dimensionless constant is independent of the composition, Equation (13) should be applicable for all the steels with AlN precipitate pinning the austenite GB. Unlike Equation (11), this model involves the initial grain size and the prediction of precipitate size. The former is altered by the chemical composition and the microstructure before the reverse transformation, and the latter may have an error in the estimation. So only satisfying Equation (13) may be dangerous for the abnormal grain growth. That means the pinning strength f_p/r_p should be significantly greater than the right-hand value of Equation (13) to ensure the avoidance of abnormal grain growth. After Equation (13), we also noticed that increasing the initial grain size was beneficial for controlling the austenite grain size during carburization. This may be a potential approach to raise the carburizing temperature or reduce the Al and N contents in gear steels, even though the initial grain size after austenitization is difficult to alter at present.

4.4. Model Validation and Application

To verify the accuracy of Equations (11) and (13), a series of additional experiments have been conducted. The carburizing temperature, time, and features of the final PAGS

are listed in Table 4. Based on the two models, the predictions were compared with the measurements in Figure 12, and several PAGSs of the verified cases are shown in Figure 13. It was seen that the accuracy rates of Equations (11) and (13) were 92% and 75%, respectively. Although the former was higher, we should note that the failure cases of Equation (13) all appeared around the critical value of f_p/r_p, which may be within the sensitive range as mentioned before. However, Equation (11) failed to predict the grain growth behavior of S1 when carburizing at 1035 °C, of which the AlN mass fraction was much larger than the threshold. In Equation (11), the ability of grain growth inhibition of S1 was the highest, while in Equation (13), it was greatly weakened due to the high carburizing temperatures. The result indicates that, if the carburizing temperature and time are close to the investigated ones in this work, Equation (11) should be preferred, because in this model, the avoidance of the estimation of precipitate ripening and the initial grain size can reduce the potential error of prediction as Figure 12 has shown. Otherwise, the variation of precipitate particle size must be considered because the mean size can be altered significantly. Then, Equation (13) is suggested. Moreover, according to the validations, the sensitive range of pinning strength can be determined to consider the change of critical pinning strength owing to the variation of initial grain size or the calculation of precipitate ripening. The upper limit of this range is suggested to be $0.03625 \cdot {d_0}^{-1.13888} + 4000\ \mathrm{m}^{-1}$.

Table 4. The pseudocarburizing conditions, the calculated states of precipitates, and features of the final PAGSs of the verified experiments.

Steel	T (°C)	t (hour)	$f_{p,m}$	r_p (nm)	f_p/r_p (m^{-1})	Existing Coarse Grains
S4	950	4	0.00017	22	20,300	No
S4	950	8	0.00017	28	16,216	No
S4	977	2	0.00015	22	18,239	Yes
S4	998	2	0.00013	26	13,666	Yes
S2	998	6	0.00019	27	18,209	No
S2	1019	6	0.00016	33	12,851	No
S2	1035	4	0.00014	34	10,964	Yes
S2	1050	2	0.00012	31	10,130	Yes
S1	998	8	0.0003	42	19,181	No
S1	1019	8	0.00027	49	14,956	No
S1	1035	4	0.00025	44	15,364	Yes
S1	1050	2	0.00023	39	15,759	No

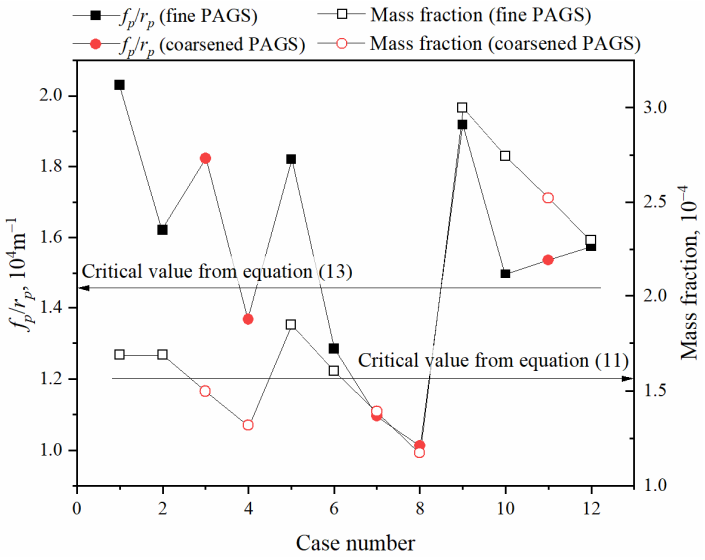

Figure 12. Calculated pinning strengths f_p/r_p (left, solid) and mass fractions (right, hollow) of the verified experiments. The cases are in the same sequence as in Table 4, and the black squares and red circles represent the fine and coarsened PAGSs, respectively.

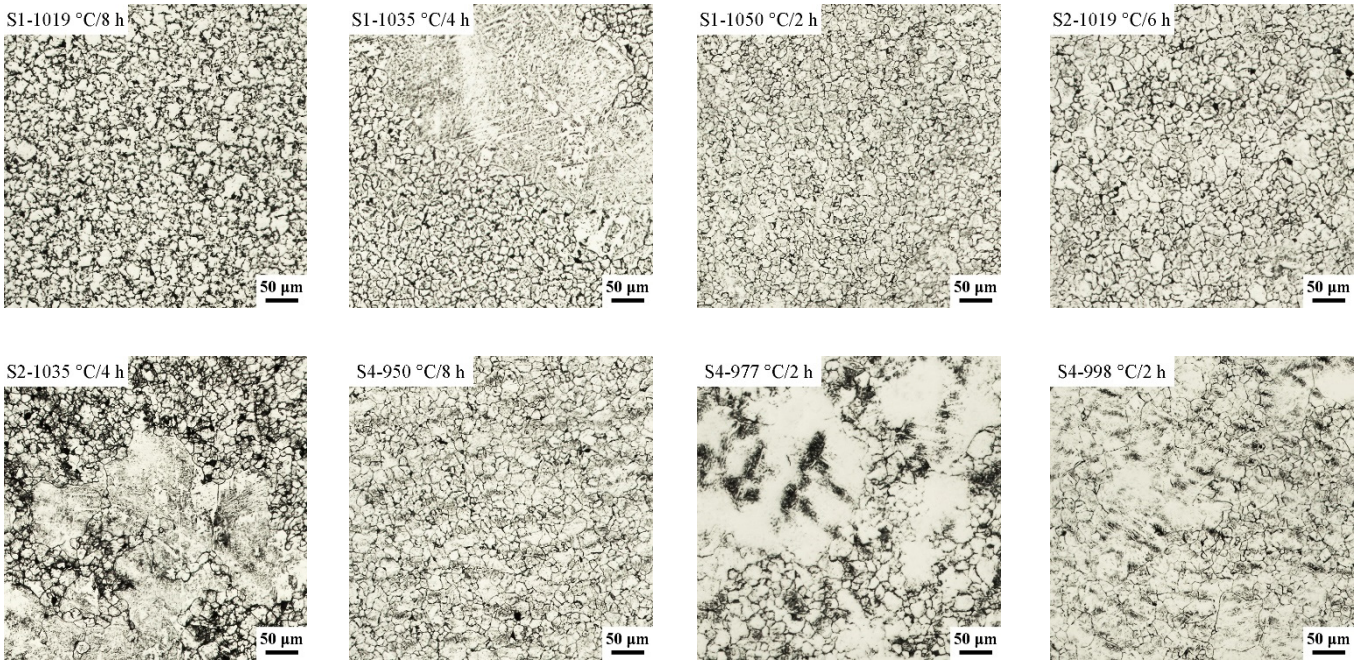

Figure 13. Several PAGSs of the verified experiments.

Using the models, we can propound the suggestion of composition modification for similar steel grades. For instance, a steel plant in China has suffered surface cracking in the continuous casting of 20Cr for a long time. The main composition of this steel is similar to the one in Table 1 and the contents of Al and N are listed in Table 5. The variation ranges of these elements allowed by the user are provided as well. It is noticed that the N content in this steel is rather high. Since the practical carburizing schedule of this steel is holding for 4 h at 960 °C, we choose Equation (11) to optimize the Al and N contents. According to the calculation of Thermo-Calc, the mass fraction of AlN at 960 °C associated with different Al and N contents is shown in Figure 14. As indicated, the AlN mass fraction of the original composition is much higher than the criterion value. We also note, however, that in the production, the steel composition and the process parameters may have slight fluctuations. So the design of Al and N contents should consider the safety distance from the critical AlN mass fraction. Using the safety distance of AlN mass fraction as 5×10^{-5}, the suggested composition is given in Table 5, which is expected to improve the hot ductility of the slab surface in continuous casting.

Table 5. The user-allowed composition range (wt.%), the original and modified composition, and the estimated third brittle zone of the commercial 20Cr steel.

Element	Allowed Range	Original	Modified
Al	0.023–0.042	0.035	0.025
N	0.011–0.021	0.018	0.012
Third brittle zone [1]		709–848 °C	718–812 °C

[1] The third brittle zone was estimated by the model from Schwerdtfeger et al. [10] with 40% as the threshold of reduction of area. Cooling rate and strain rate using 0.5 °C/s and 0.001 s^{-1}, respectively.

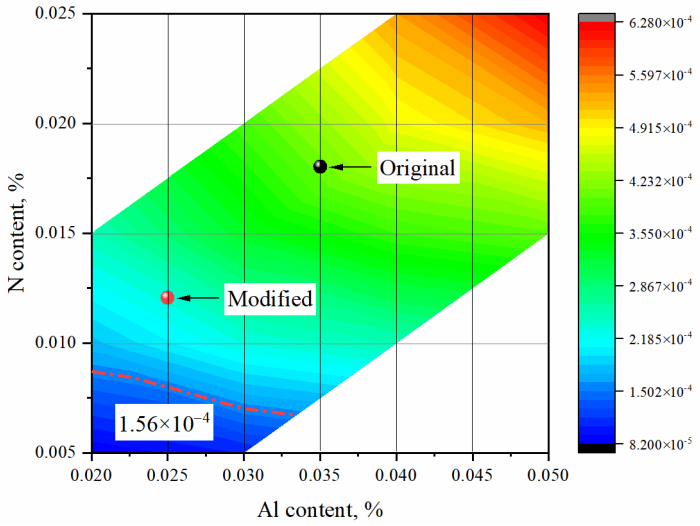

Figure 14. Calculated mass fraction of AlN precipitation at 960 °C with the variations of Al and N contents.

5. Conclusions

Aiming at the criterion for inhibiting grain coarsening in carburization, the influence of Al and N content on the austenite grain growth during carburization was investigated in this work through a series of pseudocarburizing experiments. Several conclusions can be summarized as follows.

1. The initial grain structures of carburization are close in various compositions and carburizing temperatures, of which the average size is about 12 μm. After the carburization, nearly no growth occurs if the austenite grains remain fine and uniform. However, for the cases of existing coarse grains, the fine- and coarse-grain regions are divided clearly and the coarse-grain size can be dozens of times the fine-grain size.
2. AlN precipitates provide the dominant pinning to austenite GB in the experimental steels. During the carburization, the precipitates occur the significant ripening, developing the coarse particles more than 100 nm in size and the fine particles with sizes of only tens of nm. In this process, the average particle size variation can be well simulated by the LSW theory.
3. The mass fraction and the pinning strength (defined as f_p/r_p) can determine the coarsening of austenite grain structure during carburization. In both the relationships, a critical mass fraction or a critical pinning strength was revealed, below which the PAGS will be coarsened.
4. Abnormal grain growth is the failure mode of grain size control in the carburization of gear steels. Based on the MPH simulation, the relationship between Zener pinning force and grain growth regime was constructed, and the threshold of pinning force for the abnormal grain growth was described by a power function of initial grain size. Combined with the experiment result, the dimensionless constant for the pinning of AlN on austenite GB was determined as 10.73.
5. Two models for predicting the austenite grain coarsening in carburization were constructed through the condition of abnormal grain growth. One of them concerns the mass fraction of AlN precipitates, and the other involves the variation of particle size. According to the verified experiments, the accuracies of the two models are 92% and 75%, respectively. The model which indicates the critical AlN mass fraction was used to optimize the composition of a commercial 20Cr steel associated with frequent surface cracks in production. Considering the safety distance beyond the criterion, the suggestion for reducing Al and N contents was propounded.

6. Prospects

When seeking the criterion of austenite grain coarsening, it is obvious that the determination of precipitation status, the calculation of pinning force, and the determination of pinning force conditions for abnormal grain growth act as the critical factors concerning the model accuracy. Hence, we trust that the three directions can facilitate the accuracy of the criterion in future research. First, the precise calculation about the precipitate dissolution and ripening process to reflect the distribution of particles. Second, the modified estimation of pinning force to consider the significant size difference between particles. Third, the advanced approach of introducing the pinning force in MPH simulation to produce abnormal grain growth more realistically than the present way.

Author Contributions: Conceptualization, H.L. and J.Z.; methodology, H.L. and P.L.; software, Y.D.; validation, H.L. and Y.D.; formal analysis, H.Z.; investigation, H.L. and Y.D.; resources, H.Z. and X.L.; writing—original draft preparation, H.L.; writing—review and editing, H.L. and J.Z.; visualization, P.L.; supervision, P.L. and J.Z.; funding acquisition, H.Z., H.T. and P.L. All authors have read and agreed to the published version of the manuscript.

Funding: This research was funded by National Natural Science Foundation of China, grant number U1860111 and 51874033; and Fundamental Research Funds for the Central University, grant number FRF-TP-19-017A3.

Institutional Review Board Statement: Not applicable.

Informed Consent Statement: Not applicable.

Data Availability Statement: The main data had been provided in the paper already. Any other raw/processed data required to reproduce the findings of this study are available from the corresponding author upon request.

Conflicts of Interest: The authors declare no conflict of interest.

References

1. Wang, M.Q.; Shi, J.; Hui, W.J.; Dong, H. Microstructure and mechanical properties of V-Nb microalloyed steel for heavy-duty gear. *Trans. Mater. Heat Treat.* **2007**, *28*, 18–21.
2. Białobrzeska, B.; Konat, Ł.; Jasiński, R. The influence of austenite grain size on the mechanical properties of low-alloy steel with boron. *Metals* **2017**, *7*, 26. [CrossRef]
3. Moravec, J.; Novakova, I.; Sobotka, J.; Neumann, H. Determination of grain growth kinetics and assessment of welding effect on properties of S700MC steel in the HAZ of welded joints. *Metals* **2019**, *9*, 707. [CrossRef]
4. An, J.M.; Qin, M.; Ding, Y. Effect of austenite grain size on heat treatment distortion automotive gear steels. *Heat Treat.* **2013**, *28*, 48–51.
5. Ma, L.; Wang, M.Q.; Shi, J.; Hui, W.J.; Dong, H. Rolling contact fatigue of microalloying case carburized gear steels. *Chin. J. Mater. Res.* **2009**, *23*, 251–256.
6. Ma, L.; Wang, M.Q.; Shi, J.; Hui, W.J.; Dong, H. Influence of niobium microalloying on rotating bending fatigue properties of case carburized steels. *Mater. Sci. Eng. A* **2008**, *498*, 258–265. [CrossRef]
7. Yan, B.; Liu, Y.; Wang, Z.; Liu, C.; Si, Y.; Li, H.; Yu, J. The effect of precipitate evolution on austenite grain growth in RAFM steel. *Materials* **2017**, *10*, 1017. [CrossRef] [PubMed]
8. Enloe, C.M.; Findley, K.O.; Speer, J.G. Austenite grain growth and precipitate evolution in a carburizing steel with combined niobium and molybdenum additions. *Metall. Mater. Trans. A* **2015**, *46*, 5308–5328. [CrossRef]
9. Alogab, K.A.; Matlock, D.K.; Speer, J.G.; Kleebe, H.J. The influence of niobium microalloying on austenite grain coarsening behavior of Ti-modified SAE 8620 steel. *ISIJ Int.* **2007**, *47*, 307–316. [CrossRef]
10. Schwerdtfeger, K.; Spitzer, K.H. Application of reduction of area–temperature diagrams to the prediction of surface crack formation in continuous casting of steel. *ISIJ Int.* **2009**, *49*, 512–520. [CrossRef]
11. Militzer, M.; Hawbolt, E.B.; Meadowcroft, T.R.; Giumelli, A. Austenite grain growth kinetics in Al-killed plain carbon steels. *Metall. Mater. Trans. A* **1996**, *27*, 3399–3409. [CrossRef]
12. Pous-Romero, H.; Lonardelli, I.; Cogswell, D.; Bhadeshia, H.K.D.H. Austenite grain growth in a nuclear pressure vessel steel. *Mater. Sci. Eng. A* **2013**, *567*, 72–79. [CrossRef]
13. Li, S.J.; Fan, Y.D.; Huang, S.Y. Effect of Al, Ti, Nb microalloying on mixed grain size of case-hardened steel ZF7. *Special Steel* **2013**, *34*, 52–54.
14. Ardell, A.J. The effect of volume fraction on particle coarsening: Theoretical considerations. *Acta Metall.* **1972**, *20*, 61–71. [CrossRef]

15. Kim, S.G.; Kim, D.I.; Kim, W.T.; Park, Y.B. Computer simulations of two-dimensional and three-dimensional ideal grain growth. *Phys. Rev. E* **2006**, *74*, 061605. [CrossRef] [PubMed]
16. Apel, M.; Böttger, B.; Rudnizki, J.; Schaffnit, P.; Steinbach, I. Grain growth simulations including particle pinning using the multiphase-field concept. *ISIJ Int.* **2009**, *49*, 1024–1029. [CrossRef]
17. Kim, J.M.; Min, G.; Shim, J.H.; Lee, K.J. Effect of time-dependent pinning pressure on abnormal grain growth: Phase field simulation. *Met. Mater. Int.* **2018**, *24*, 549–559. [CrossRef]
18. Kang, Y.; Yu, H.; Fu, J.; Wang, K.; Wang, Z. Morphology and precipitation kinetics of AlN in hot strip of low carbon steel produced by compact strip production. *Mater. Sci. Eng. A* **2003**, *351*, 265–271. [CrossRef]
19. Cheng, L.M.; Hawbolt, E.B.; Meadowcroft, T.R. Modeling of dissolution, growth, and coarsening of aluminum nitride in low-carbon steels. *Metall. Mater. Trans. A* **2000**, *31*, 1907–1916. [CrossRef]
20. Wang, F.; Davis, C.; Strangwood, M. Grain growth behaviour on reheating Al–Nb-containing steel in the homogenised condition. *Mater. Sci. Technol.* **2018**, *34*, 587–595. [CrossRef]
21. Cahn, J.W. The impurity-drag effect in grain boundary motion. *Acta Metall.* **1962**, *10*, 789–798. [CrossRef]
22. Rudnizki, J.; Zeislmair, B.; Prahl, U.; Bleck, W. Prediction of abnormal grain growth during high temperature treatment. *Comput. Mater. Sci.* **2010**, *49*, 209–216. [CrossRef]
23. Kim, S.G.; Park, Y.B. Grain boundary segregation, solute drag and abnormal grain growth. *Acta Mater.* **2008**, *56*, 3739–3753. [CrossRef]
24. Di Nunzio, P.E. A discrete approach to grain growth based on pair interactions. *Acta Mater.* **2001**, *49*, 3635–3643. [CrossRef]
25. Rios, P.R.; Fonseca, G.S. Geometrical models for grain, grain boundary and grain edge average curvature in an Al-1mass%Mn alloy. *Scripta Mater.* **2005**, *52*, 893–897. [CrossRef]
26. Dépinoy, S.; Marini, B.; Toffolon-Masclet, C.; Roch, F.; Gourgues-Lorenzon, A.F. Austenite grain growth in a 2.25Cr-1Mo vanadium-free steel accounting for Zener pinning and solute drag: Experimental study and modeling. *Metall. Mater. Trans. A* **2017**, *48*, 2289–2300. [CrossRef]
27. Nes, E.; Ryum, N.; Hunderi, O. On the Zener drag. *Acta Metall.* **1985**, *33*, 11–22. [CrossRef]
28. Rios, P.R. Overview no. 62: A theory for grain boundary pinning by particles. *Acta Metall.* **1987**, *35*, 2805–2814. [CrossRef]